ACS APPLIED MATERIALS & INTERFACES

www.acsami.org
Research Article

Photoelectrochemical Two-Dimensional Electronic Spectroscopy (PEC2DES) of Photosystem I: Charge Separation Dynamics Hidden in a Multichromophoric Landscape

Manuel López-Ortiz,[▽] Luca Bolzonello,[▽] Matteo Bruschi, Elisa Fresch, Elisabetta Collini, Chen Hu, Roberta Croce, Niek F. van Hulst,* and Pau Gorostiza*

Cite This: ACS Appl. Mater. Interfaces 2024, 16, 43451−43461
Read Online

ACCESS | Metrics & More | Article Recommendations | Supporting Information

ABSTRACT: We present a nonlinear spectroelectrochemical technique to investigate photosynthetic protein complexes. The PEC2DES setup combines photoelectrochemical detection (PEC) that selectively probes the protein photogenerated charges output with two-dimensional electronic spectroscopy (2DES) excitation that spreads the nonlinear optical response of the system in an excitation−detection map. PEC allows us to distinguish the contribution of charge separation (CS) from other de-excitation pathways, whereas 2DES allows us to disentangle congested spectral bands and evaluate the exciton dynamics (decays and coherences) of the photosystem complex. We have developed *in operando* phase-modulated 2DES by measuring the photoelectrochemical reaction rate in a biohybrid electrode functionalized with a plant photosystem complex I−light harvesting complex I (PSI-LHCI) layer. Optimizing the photoelectrochemical current signal yields reliable linear spectra unequivocally associated with PSI-LHCI. The 2DES signal is validated by nonlinear features like the characteristic vibrational coherence at 750 cm^{-1}. However, no energy transfer dynamics is observed within the 450 fs experimental window. These intriguing results are discussed in the context of *incoherent mixing* resulting in reduced nonlinear contrast for multichromophoric complexes, such as the 160 chlorophyll PSI. The presented PEC2DES method identifies generated charges unlike purely optical 2DES and opens the way to probe the CS channel in multichromophoric complexes.

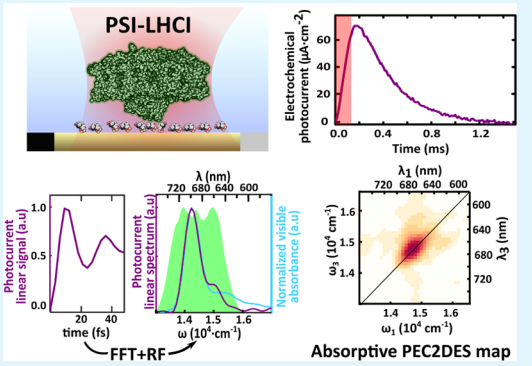

KEYWORDS: *protein electronic spectroscopy, photosynthetic electron transport chain, chlorophyll, photoelectrochemical sensor, redox mediator, incoherent mixing*

INTRODUCTION

Photosynthesis is the process that underlies the transformation of photonic to chemical energy in subsequent steps of time scales spanning 10 orders of magnitude. The first step is photon absorption followed by excitation energy transfer (EET) in the femto/picosecond time scale. Excitons migrate to the reaction center (RC), where charge separation (CS) occurs in picoseconds.[1] Electrons are then transferred to opposite sides of the membrane embedding the RC in a series of electron transfer (ET) steps that last from tenths of picoseconds to hundreds of nanoseconds[2] and foster the photosynthetic electron transport chain that supports chemical synthesis at the scale of seconds.

To study photosystem complexes, it is crucial to combine results from different approaches like genetics, physiology, structural biology, theoretical calculations, and magnetic and optical spectroscopies.[3] Further benefits are obtained when multiple techniques are applied simultaneously such that chemical, electronic, or optical signatures are detected at the same time. For example, combinations of electrochemical and optical spectroscopy methods have been developed, like Raman[4,5] including surface- and tip-enhanced, transient absorption,[6] X-ray,[7] FTIR,[7] and confocal fluorescence.[8−10] Each spectroelectrochemical technique poses specific challenges and offers unique advantages to study reactions in static and dynamic conditions (*in situ* and *operando*, respectively).[11−14]

Understanding the subtle details that regulate natural photosynthesis has allowed developing artificial[15,16] and *de novo* designed proteins.[17] The spectral absorption of photosynthetic complexes has been engineered by introducing synthetic dyes[18,19] or assembling chimeras of photosynthetic and light-harvesting complexes from different organisms.[20] In

Received: March 28, 2024
Revised: July 26, 2024
Accepted: August 2, 2024
Published: August 9, 2024

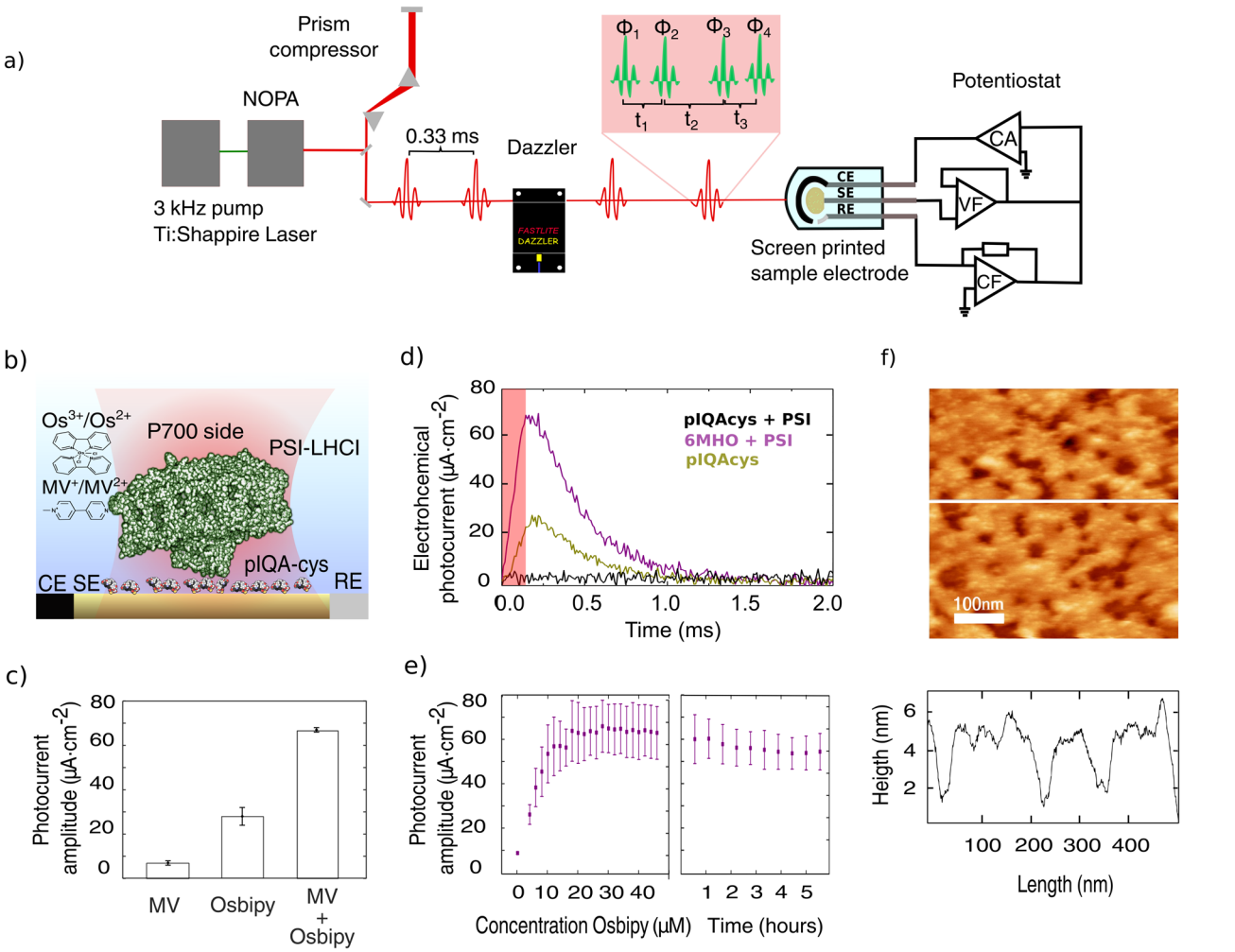

Figure 1. Photoelectrochemical current response of Au-pIQA-cys-PSI-LHCI electrodes. (a) Experimental setup for photoelectrochemical current detected 2DES. Pulse generation and shaping performed by pump laser, NOPA, and acousto-optic modulator (Dazzler) are shown on the left. Four-pulse excitation scheme with phases Φ_{1-4} and relative pulse delay t_{1-3} is shown in the red inset. Photoelectrochemical current-detection system is depicted on the right side including the potentiostat scheme (CF: current follower, VF: voltage follower, and CA: current amplifier) and sample miniaturized screen-printed electrode (CE: counter electrode, SE: sample electrode, and RE: reference electrode). (b) Cartoon representation of transparent Au electrode functionalized with pIQA-cys peptide linker orienting PSI-LHCI complexes that expose the P700 luminal side to the electrolyte. (c) Photochrono-amperometry of Au electrodes (at −50 mV w.r.t. to silver pseudoreference electrode) incubated with pIQAcys and PSI (purple trace, maximal photoresponse) and functionalized with mercaptohexanol (MHO) and PSI (brown trace, lower photoresponse) and pIQAcys alone (black trace, no photoresponse). Electrolyte solution contains PBS 50 mM pH 7.4, MV 200 mM, and osbipy 20 μM. The red shaded area represents an irradiation pulse of 125 μs with a power of 35.7 mW·cm^{-2} and a wavelength centered at 690 nm. Traces represent the average of eight consecutive pulses. (d) Photoelectrochemical current transient amplitude for Au-pIQA-cys-PSI-LHCI with MV (200 mM), osbipy (20 μM), and MV + osbipy. (e) Photoelectrochemical current transient amplitude versus osbipy concentration and time evolution of transient photoelectrochemical current amplitude under constant pulsed irradiation. Error bars in panels d and e represent the standard error for n = 3 independent experiments. (f) AFM characterization of PSI-pIQA-cys-Au films attached to Au electrodes. Scan size of 500 × 500 nm and a vertical axis color scale were set to 10 nm amplitude. The height profile corresponds to the white line in the scan. Scan image threshold results in an approximate surface coverage of ∼75%.

natural and artificial systems, higher absorption results in higher overall efficiency only if excitons can be trapped by the reaction center and CS takes place. To decipher photosynthetic complexes and engineer novel photosynthetic strategies, it is thus key to probe the EET pathways leading to CS. Thus, we aimed to isolate and detect only the nonlinear spectroscopy features associated with CS excitons. To do so, we optimized a photoelectrochemical (PEC) current detection method to perform spectroscopic measurements of photosystem complexes.

The multichromophoric structure of photosystem complexes and the ultrafast absorption, EET, and CS rates[21,22] pose challenges to track photosynthetic exciton dynamics in time, space, and energy and to interpret the experimental results, which often requires computational chemistry calculations. In this sense, the advent of two-dimensional electronic spectroscopy (2DES) helped to disentangle congested spectral bands by spreading out nonlinear optical signals in excitation−detection maps. Indeed, 2DES provides a detailed picture of homogeneous and inhomogeneous broadenings, spectral diffusion, energy transfer, correlations between excited states, and vibrational and electronic coherences, thus encompassing the entire excited-state dynamics.[23] Yet, even 2DES dynamics of photosynthetic systems can be inconclusive and con-

https://doi.org/10.1021/acsami.4c03652
ACS Appl. Mater. Interfaces 2024, 16, 43451−43461

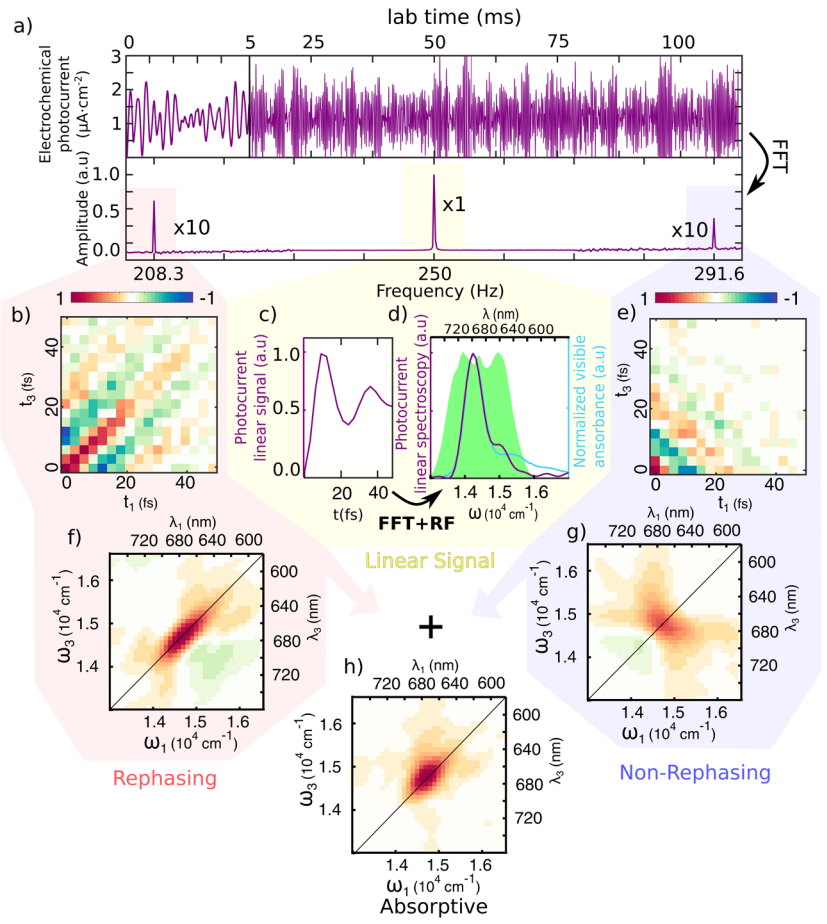

Figure 2. (a) Top: Photoelectrochemical current readout from the potentiostat (first 5 ms magnified) with periodic modulation of the phase performed at fixed delay times between pulses. Bottom: Fourier transform revealing linear, rephasing, and nonrephasing signals at different modulation frequency combinations. (c) Linear signal extracted from the first pulse pair as a function of delay time t_1 and averaged over the other times, acquired in the rotating frame (RF). (d) Comparison of the Fourier transform of the signal (purple, shifted by RF) with the absorption spectrum of the PSI (light blue) and the laser spectrum used for the experiment (green shaded area). (b, e) Time reconstruction of rephasing and nonrephasing signal into t_1−t_3 maps (shown at t_2 = 100 fs). Their Fourier transforms produce the ω_1−ω_3 maps (f, g) used for data interpretation. The sum of these maps leads to the absorptive map (h).

troversial[24] and thus requiring novel function-oriented spectroscopical methods.

To develop photoelectrochemical two-dimensional electronic spectroscopy (PEC2DES), we have optimized the photoelectrochemical current amplitude and kinetics of a photosystem protein complex tethered to an electrode under potentiostatic control. This "action" spectroscopy technique probes the CS functionality of photosynthetic complexes and the distinct ET processes leading to CS. To validate this method, we have employed plant photosystem complex I−light harvesting complex I (PSI-LHCI) as model system. In PSI-LHCI, light harvesting by the antenna chlorophylls is used to drive the CS in the RC.

The final observable in conventional fully noncollinear 2DES experiment is the nonlinear optical polarization,[25−27] i.e., a coherent electric field generated by the sample interacting with a sequence of exciting laser pulses. Instead, collinear 2DES[28−31] readout does not rely on electric field detection but on any observable proportional to the excited-state population after interaction with the excitation pulses. For example, if the system is luminescent, fluorescence is a convenient readout that allows quantifying the excited-state population within ultrafast spectroscopy.[32−37] However, despite its reported advantages to study photosynthesis, fluorescence relaxation is a loss channel; i.e., it does not directly probe the productive pathway leading to CS and chemical synthesis. By definition, CS is a nonradiative decay channel, and excitons reaching the RC and undergoing CS do not generate any fluorescence signal. CS initiates a series of ET processes from the chlorophyll special pair (P700) to the terminal electron donor, the iron sulfur cluster (F_B) at the stromal side of the membrane. The PSI-LHCI redox cofactors $P700^+$ and F_B^- are then reduced and oxidized by soluble redox protein partners plastocyanin and ferredoxin, respectively, thereby coupling PSI-LHCI to the photosynthetic electron transport chain. Thus, we reasoned that draining charges from PSI-LHCI redox cofactors would yield an electrochemical current that could be exploited as a 2DES readout *in vitro*. In our experimental approach, the photoelectrochemical current directly measures the outcome of PSI-LHCI light harvesting, i.e., electrical charges mobilized in the photosynthetic electron transport chain. Using the higher plant *Arabidopsis thaliana* PSI-LHCI, we recorded for the first time PEC2DES in photosynthetic complexes.

https://doi.org/10.1021/acsami.4c03652
ACS Appl. Mater. Interfaces 2024, 16, 43451−43461

EXPERIMENTAL METHODS

Photoelectrochemical Current Readout of PSI-LHCI Samples. In optical measurements of isolated PSI-LHCI complexes, exogenous electron donors were introduced to boost ET kinetics of the photo-oxidized state (F_B/P700$^+$) and closed state (F_B^-/P700) toward the open state (F_B/P700), thus allowing the RC to separate new charge pairs upon successive excitations and preventing P700$^+$ from quenching excitation.[38] The fraction of closed RC thus depended on the reducing agent concentration and the number of absorbed photons by each PSI-LHCI. For instance, Wientjes and Croce report a lifetime of ∼30 ms for P700$^+$ and an RC closed state fraction of 78% in the presence of 10 mM NaAsc and 10 μM PMS for a light intensity of 531 μE·m^{-2}·s^{-1} (estimated fluence 128 photons·s^{-1} per PSI).[39] Despite the 78% population of the closed state, the authors conclude that the trapping efficiency and lifetime are marginally affected by the P700/F_B oxidation state due to the effective quenching of excitations by P700$^+$.[39] In contrast, in the photoelectrochemical readout, the signal is proportional to PSI-LHCI photogenerated charges; therefore, P700$^+$ and F_B^- must be reduced and oxidized, respectively, to the open state (F_B/P700) before the next photoexcitation pulse to preserve the photoelectrochemical yield.[40] Efficient ET with the charge exchange cofactors is thus a requisite to restore P700$^+$ and F_B^- back to the open state at a higher rate than that for excitation pulse-train repetition. In the same way, increasing the reduction and oxidation rates of P700$^+$ and F_B^- back to the open state at a higher rate than that for excitation pulse-train repetition. In the same way, boosting the ET of P700$^+$ and F_B^- rates with the electrode via exogenous mediators, fosters the photoelectrochemical current signal amplitude that is desirable to attain a signal-to-noise ratio sensitive to nonlinear effects.

To maximize photoelectrochemical current output, soluble redox mediators that can exchange charge with P700$^+$ and F_B^- were employed. For the electron acceptor (hole donor) side of PSI, we used osmium bis-2,2′-bipyridine chloride (osbipy) to take advantage of the lower formal potential (higher energy) of osbipy compared to P700$^+$. Osbipy has been previously used as redox mediator for PSI-based biohybrid electrodes cross-linked to redox polymers[41−44] or diluted into electrolyte.[42] Regarding the PSI electron donor side, we chose methyl viologen (MV) as electron acceptor of the high energy electrons of F_B^-. MV is a redox active heterocyclic molecule used as herbicide due to its ability to oxidize F_B^- and donate electrons to O_2, thus disrupting the photosynthetic electron transport chain and facilitating the formation of reactive oxygen species (ROS).[45,46] In an electrochemical cell, however, electrodes readily oxidize the MV$^{+\cdot}$ radical formed upon F_B^- oxidation, thus enhancing ET rates and limiting the formation of ROS.[47] Simultaneous reduction of osbipy and oxidation of MV in the sample electrode result in partially canceling currents, but because the oxidation and reduction rates of the mediators are not exactly equal, they give rise to a transient photoelectrochemical current.[48,49] Although this configuration leads to low stationary currents, we took advantage of submillisecond electrochemical transient responses to perform spectroscopic recordings at kHz laser repetition rates.

The photoelectrochemical current was recorded under potentiostatic control (Metrohm Autolab) making use of Au transparent screen-printed electrodes (Metrohm Dropsens) (Figure 1a) harbored in a customized electrochemical cell adapted for spectroscopic experiments (Figure SI-F3). Purified PSI-LHCI complexes (see Supporting Information SI1) were functionalized using pIQAcys linker peptide[50] exposing the P700 luminal side to the electrolyte (Figure 1b and Supporting Information SI2). PSI-LHCI functionalization, orientation, working electrochemical window, and scanning probe characterization were reported in a previous work.[51] Briefly, we applied a constant potential of −50 mV to trade off high photocurrents while preserving the stability of the sample over the hours of PEC2DES recordings.

Phase Modulation and 2DES Parameters. For effective and rapid photoelectrochemical current-detected 2DES, we exploited our recently developed pulse-by-pulse shaping with collinear laser setup.[31] Briefly, a 3 kHz amplified Ti/sapphire laser (Coherent Libra) generates a continuous pulse train centered at 800 nm, which is converted and broadened (green area in Figure 2d) through a commercial but home-modified NOPA (Light Conversion TOPAS White). A prism compressor was used to roughly precompensate the phase dispersion, and finally, an acousto-optical pulse shaper (Dazzler) finely adjusted the phase for reaching transform-limited pulse (∼10 fs, see Figure SI-F4) and generated four-pulse replicas with control on their mutual time delay and phase (Supporting Information SI5). The time delays between the first and second pair of pulses (t_1 and t_3) set the excitation and detection frequencies ($\omega_1$and ω_3), respectively (Figure 1a), whereas the population time t_2 fixes the time interval between excitation and detection pairs. In this so-called "action" 2DES, phases of individual pulses (Φ_{1-4}) were modulated in time and used to separate the different components of the spectroscopic response of the system. In particular, rephasing and nonrephasing responses fell into distinct peaks in the frequency domain (Figure 2a, bottom).[28] Additional technical details of the experiment are presented in Supporting Information SI4 and SI5.

RESULTS AND DISCUSSION

Photoelectrochemical and AFM Characterization of Au-pIQAcys-PSI-LHCI Samples. Prior to the integration of electrochemical and 2DES setups (Figure 1a), the photoelectrochemical current transient signal of Au-pIQAcys-PSI-LHCI samples was characterized with LED pulses. An example of a photoelectrochemical current trace upon illumination with 125 μs pulses is shown in Figure 1c (purple trace). Photoelectrochemical current responses are lower if PSI-LHCI is incubated on a mercaptohexanol self-assembled monolayer (Figure 1c, brown trace). Control experiments in the absence of PSI-LHCI (Figure 1c, black trace) and heat-denatured PSI-LHCI samples (1 h at 60 °C) exhibit negligible photoelectrochemical current. In addition, the linear component of PEC2DES (*vide infra*), that is, the electrochemical current linear spectrum shown in Figure 2d, overlaps with the PSI-LHCI absorption peak, supporting that the photoelectrochemical current is due to PSI-LHCI photocatalytic activity.

The addition of 20 μM osbipy mediator to the working buffer (phosphate buffer saline (PBS), 50 mM, pH 7.4) was sufficient to observe transient photoelectrochemical currents upon pulsed illumination with a 28 ± 4 μA·cm^{-2} amplitude (Figure 1d). On the other hand, the buffer solution containing MV exclusively (200 mM) exhibits a 4-fold lower photoelectrochemical current amplitude of 7 ± 1 μA·cm^{-2}. In the presence of both mediators, the photoelectrochemical current amplitude rises to 67 ± 1 μA·cm^{-2} (Figure 1c,d), exhibiting a time decay constant of 0.27 ± 0.02 ms. To optimize the osbipy concentration, the photoelectrochemical current amplitude was evaluated with an excess (200 mM) of MV for increasing osbipy concentration (Figure 1e) and we observed saturating photoresponses above 20 μM osbipy. Sample stability was evaluated by measuring the photoelectrochemical current under pulsed illumination for several hours. Figure 1e shows that sample stability allows measuring several 2DES maps without significant sample degradation (i.e., photoelectrochemical current reduction).

AFM scans of Au-pIQA-cys-PSI-LHCI electrodes (Figure 1f and Supporting Information SI3) reveal a submonolayer deposition with ∼5 nm height, consistent with PSI crystallographic size and previously reported heights of PSI samples absorbed on gold electrodes.[42] Scans reveal an approximate surface coverage of ∼75% that corresponds approximately to 1.7 × 10^{10} PSI-LHCI complexes on the surface of the

https://doi.org/10.1021/acsami.4c03652
ACS Appl. Mater. Interfaces 2024, 16, 43451−43461

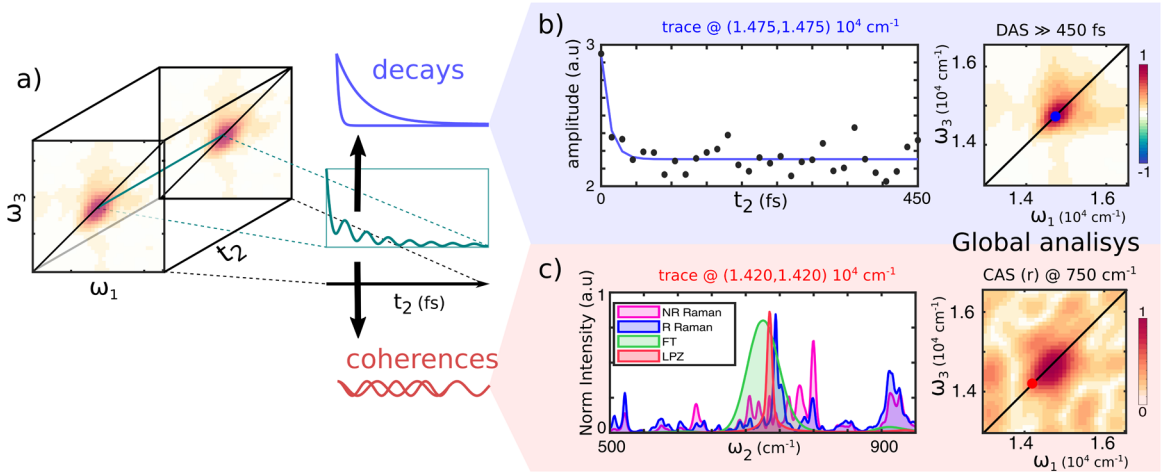

Figure 3. (a) Schematic illustration of 2DES data. The nonlinear signal along t_2 is a sum of different decaying or oscillating contributions. (b) Signal decay trace along t_2 extracted at the peak's maximum, $\omega_1 = \omega_3 = 14{,}750$ cm^{-1} (scatter), and its global fit (blue line). After the initial ultrafast decay, the signal evolution is flat. The lack of signal evolution is confirmed at every coordinate by the 2D-DAS from the global fitting with a characteristic time much longer than the experimental range. (c) An analysis of the residuals of the global fitting shows the presence of structured oscillations in the signal. The FFT (green) and linear predictor Z-transforms[27] (LPZ, red) applied to the residuals of the global fitting highlight the presence of an oscillation at 750 cm^{-1}. The same frequency component appears in the resonant (blue) Raman spectrum, whereas it is less evident in the nonresonant (pink) one (633 and 514 nm laser excitation, respectively) of chlorophyll *a* in ethanol, suggesting that this component comes from vibrational coherences of the molecule. The 750 cm^{-1} component is also retrieved from the global fitting with oscillating functions, returning a 2D-CAS map (right) with an intensity distribution like the one in the 2D-DAS.

electrode. Neglecting recombination and partially canceling currents from the redox mediators, the electrode current is associated with the number of photogenerated charges, and we can estimate a lower bound of the fraction of PSI-LHCI complexes that yield photocurrent.[40] The total charge is computed by integrating the photoelectrochemical current signal over a single pulse, revealing that ∼40% of PSI-LHCI complexes provide a charge pair at every pulse.

PEC2DES Results. The amplitude of the photoelectrochemical current signal upon illumination with laser phase-modulated four-pulse trains is shown in Figure 2a (top). Linear, rephasing, and nonrephasing peaks in the frequency domain are shaded in yellow, red, and blue, respectively (Figure 2a, bottom). The linear (Figure 2c) and nonlinear signals (Figure 2b,e) can then be reconstructed as a function of the delays t_1−t_3 between pulses. By Fourier transforming the delays, we then obtain the linear (Figure 2d) and 2DES spectra (Figure 2f,g), that is, the response maps of the sample excited at frequency ω_1 and detected at frequency ω_3.

The linear spectrum obtained with this method overlaps with the optical absorption spectrum of PSI (Figure 2d), thus validating our approach. The absorptive 2D map (Figure 2h) obtained by summing the rephasing and nonrephasing signals shows a single broad peak centered at 14,750 cm^{-1} (678 nm), which corresponds to the main absorption transition of the PSI.

Global Analysis of PEC2DES Data. 2DES spectra are recorded for increasing excitation−detection delays (t_2), allowing tracking of the excited-state populations dynamics. The analysis of the signal evolution as a function of the population time t_2 has been performed using a complex multiexponential global analysis[52] to identify the main temporal components. The amplitudes associated with real (decays) and complex (oscillations) exponential functions that globally fit the data are retrieved to generate decay-associated spectra (2D-DAS) and coherence-associated spectra (2D-CAS) maps respectively (Figure 3). These maps depict the amplitude distribution of every temporal component on the excitation−detection axis, which is particularly convenient to ease the visualization of the response evolution.

The global fit, using only real exponentials, returns two 2D-DAS components with time constants of 10 and ≫450 fs. The fastest 2D-DAS component is generated by the pulse overlap around $t_2 = 0$, which gives rise to a spurious signal[53] and is not considered for the analysis. Instead, the second 2D-DAS, shown in Figure 3b (right), associated with ≫450 fs component captures dynamic processes evolving in a time scale longer than the investigated time window. The signal distribution in the 2D-DAS of Figure 3b is similar to any map along t_2, indicating that during the first 450 fs, the 2DES maps do not significantly change shape or intensity. An example of the signal evolution along t_2 is displayed in Figure 3b (left), with the signal extracted at the peak's maximum.

Applying Fourier transform to the residuals of the fittings along t_2, it reveals a prominent peak with a frequency around 750 cm^{-1} (Figure 3c, left), suggesting the presence of coherent behavior. To verify the effective significance of this beating, we performed again the global fit procedure, also including an oscillating component. The same frequency component is retrieved. The amplitude distribution associated with this coherence component is represented in 2D-CAS depicted in Figure 3c (right). The 2D-CAS shows that this beating component contributes mainly at coordinates close to the peak maximum although slightly red-shifted.

Interestingly, this beating component does not show the typical off-diagonal pattern expected for vibrational coherences.[54] However, we noted the overlap of a 750 cm^{-1} mode between the FFT or LPZ spectral analysis[55] on residuals (picked at $\omega_1 = \omega_3 = 14{,}500$ cm^{-1} ≈ 690 nm) with resonant Raman spectra (Figure 3c, left) of chlorophyll *a* (the main chromophore in PSI-LHCI complex). The resonant condition of Raman reveals an enhancement of Raman scattering at 750 cm^{-1}, suggesting the coupling of a vibrational mode with such energy to the optical transition. It is thus likely that the

https://doi.org/10.1021/acsami.4c03652
ACS Appl. Mater. Interfaces 2024, 16, 43451−43461

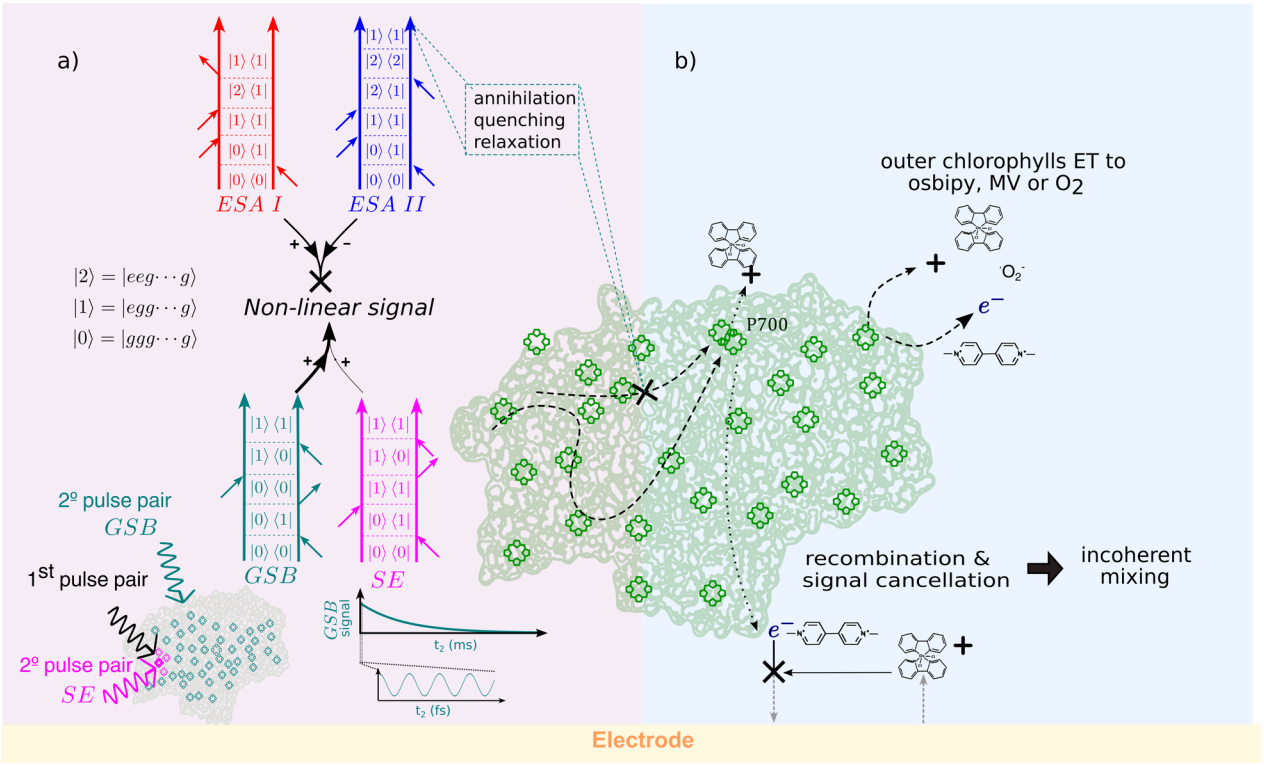

Figure 4. Diagram showing the possible causes for the lack of dynamics in PEC2DES, including differences in excitation scheme (a) on the left side and electrochemical detection (b) on the right side of the panel. (a) Four-pulse excitation. Feynman pathways describing four-pulse excitation are excited-state absorption ESA I (red), ESA II (blue), stimulated emission SE (magenta), and ground-state bleaching GSB (aquamarine). Even if ESA II would generate two excitons in the same protein after the four-pulse interaction, annihilations or limited CS will reduce the detection to one charge, as much as ESA I. Having opposite signs, the two ESA contributions cancel out, and the nonlinear signal will be given only by SE and GSB pathways. The SE signal is associated with chlorophylls that are excited by both the first pulse pair (black) and second pulse pair (magenta), whereas the GSB signal is associated with non-previously excited chlorophylls (aquamarine). The GSB signal decays in the millisecond time scale, in an experimental window (zoom for ~500 fs) where only coherences are expected from GSB contribution. (b) Electrochemical detection. CS might take place in outer chlorophylls other than P700 transferring charge to MV resulting in ultrafast dynamics of single or few chlorophylls instead of the PSI-LHCI complex. Recombination of charges in the electrochemical solution before the detection and signal cancellation in the electrode could give rise to the so-called "incoherent mixing" where part of the linear signal leaks into the nonlinear signal.

oscillation detected in the 2DES is the same nuclear mode enhanced in resonant Raman.[22,56]

Incoherent Mixing and the Absence of Population Dynamics. The overlap between the photoelectrochemical current-detected linear spectrum and the absorption spectrum (Figure 2d) demonstrates that the detected electrons are photogenerated by the PSI-LHCI complexes. Moreover, the oscillation found in the PEC2DES maps along t_2 is an ubiquitous feature of time-resolved spectra of chlorophyll *a*, and in addition to our resonant Raman spectra, it was found in 2DES experiments of the PSII reaction center[22] and free-chlorophyll samples.[56−59] These observations suggest that the photoelectrochemical current-detected 2DES is sensitive to both linear and nonlinear spectroscopic features of PSI-LHCI and provides experimental access to an observable that was not available previously.

Remarkably, the PEC2DES results do not exhibit either population dynamics or spectral diffusion within our experimental time range as the evolution of the PEC2DES maps is essentially flat. This behavior contrasts with the subpicosecond kinetics obtained from the previously reported nonlinear optical response of plant PSI-LHCI obtained with a conventional optical readout.[60−63] Indeed, the global analysis of optically detected 2DES results revealed a ~ 250 fs component associated with excited-state equilibration and transfer to the bulk chlorophylls[60] in PSI-LHCI extracted from spinach leaves, whereas Akthar et al. reported an exciton relaxation time in the core antenna of 500 fs.[61] Similar 2DES experiments in algae[63] and cyanobacteria[62] reveal subpicosecond exciton equilibration and trapping kinetics ranging from 1 to 20 ps.

In light of these previous results, the absence of ultrafast dynamics in our photocurrent measurements might appear surprising. However, the distinct methods of excitation and detection in PEC2DES compared to standard 2DES can explain why oscillations, but not population dynamics or spectral diffusion, are observed in the former. In particular, the differences between four-pulse and three-pulse excitation and photoelectrochemical current with respect to optical detection are discussed below and illustrated in Figure 4.

Optically detected 2DES and action-detected 2DES probe the third-order polarization and the fourth-order excited-state population induced by the laser pulses, respectively.[64,65] In both techniques, the signal can be rationalized using Feynman diagrams, representing the pathways followed by the system upon light−matter interaction.[66] These pathways can be distinguished into ground-state bleaching (GSB), stimulated emission (SE), and excited-state absorption (ESA), as depicted in Figure 4a. In action detection, two kinds of ESA pathways are possible: ESAI ending in a one-exciton population, i.e., one

https://doi.org/10.1021/acsami.4c03652
ACS Appl. Mater. Interfaces 2024, 16, 43451−43461

molecule excited, and ESAII ending in a two-exciton population, i.e., two molecules excited.[65,67−70] Having opposite signs, the two kinds of ESA pathways can interfere destructively in the spectrum, eventually leading to the partial or complete cancellation of the associated spectral features.

According to the nonlinear response theory, the amplitude of fourth-order pathways scales with the fourth power of the transition dipole moment and is additionally weighted by the quantum yield (QY) of the final excited-state population, i.e., the number of CS events it can lead to.[67,69,70] The extent of ESA cancellation strictly depends on the relative quantum yield (QY) between two- and one-exciton states.[67,69] In an ideal scenario, the QY of two-exciton states would be twice that of one-exciton states, meaning that every exciton will lead to a CS event. In this case, action-detected 2DES gives results analogous to those of the optically detected technique. However, in realistic situations, the presence of alternative pathways other than CS involving two-exciton states can reduce their QY, and the ESA contribution begins to cancel out. In the limiting case of one- and two-exciton states having the same QY, ESA pathways completely cancel out in the spectra, and the nonlinear signal simply reduces to the sum of GSB and SE pathways.

In the case of the PSI-LHCI complex, we identified two different mechanisms that reduce the QY of two-exciton states. The first is the exciton−exciton annihilation (EEA), which is a known process affecting the signal in action-detected 2DES.[65,67,68] In EEA, the interaction between excitons located on different chromophores results in the net loss of an exciton upon encounter. The second is the limited number of CS events at the RC.[70] When the RC is occupied by an exciton, it switches from an *open* state to a *closed state*, preventing the trapping of another exciton.

In photosystem complexes, diffusion-limited EEA can compete with exciton trapping at the RC occurring on the same picosecond time scale.[71] Because of its power dependence, EEA can be mitigated using lower laser fluences. Nevertheless, the generation of a two-exciton state population is intrinsic to the fourth-order light−matter interaction. Therefore, it is difficult to completely avoid EEA in action-detected 2DES. However, we expect that the main mechanism affecting the signal is the limited number of CS events. Because the exciton lifetime (∼ns) is much shorter than the RC turnover (∼ms), in PSI-LHCI, only one exciton will lead to a CS event, whereas the other recombines independently. Consequently, after each sequence of laser pulses, only one CS per photosystem complex is detected in PEC2DES. This fact limits the QY of two-exciton states to be equal to that of one-exciton states.

All of these mechanisms introduce nonlinearities in the signal other than the optical one. This kind of nonlinearities leads to the so-called *incoherent mixing*, where part of the linear signal mixes during the detection, entering the nonlinear signal.[69,70,72,73] To estimate the amount of incoherent mixing in the spectrum, we assume that one- and two-exciton states have the same QY based on the above justifications. In this case, ESA cancellation is complete, and the nonlinear signal is given by the sum of GSB and SE contributions. The relative weights of SE and GSB pathways depend on the number of chromophores sharing the same RC. After the first pulse pair has interacted with a chromophore, the weight of the SE contribution is proportional to the probability that the second pulse pair will interact again with the same chromophore, whereas that of the GSB contribution is related to the probability of interacting with both the same and a different chromophore.[70] In our specific experimental conditions, the laser fluence is set such that each pulse pair excites on average about one chlorophyll per PSI-LHCI complex. Therefore, the second pair will more likely excite a different chlorophyll (∼160 chlorophylls) rather than interact again with the same one. Following this argument, the contribution of SE is negligible (160-fold smaller) compared to that of GSB, which, in this case, is the main pathway in the PEC2DES signal.

Note that most of the GSB pathways result from the excitation of two different chromophores and, therefore, are equivalent to the product of two linear signals.[69,70] The dominant contribution of GSB and its linear character explain the absence of population dynamics during t_2 in the PEC2DES spectra and the broad line shape of the peak. Instead, the origin of the oscillatory component and why it appears on top of the incoherent mixing require further investigation. However, its frequency is compatible with a ground-state vibrational mode of chlorophylls around 750 cm^{-1}.

Recently, the reduced contrast in the energy transfer dynamics along t_2 has also been reported in the fluorescence-detected 2DES of the LH2 complex.[74] The authors explain that the ratio between SE and GSB contribution in the 2D spectra depends not only on the number of chromophores[70] but also on the presence of delocalization between them. Therefore, delocalization can effectively act in reducing the incoherent mixing contribution through dipole moment redistribution between excitonic states.[74]

On the other hand, redox mediators employed to drain charges from the terminal electron donor/acceptor cofactors could partially penetrate the PSI-LHCI protein matrix and directly drain charges from outer chlorophylls, preventing migration to RC (Figure 4b). It has been recently reported that a quinone mediator (DCBQ) modifies the transient absorption features at 715 and 685 nm in cyanobacterial cells and isolated photosystem I complexes in the picosecond time scale.[75] The authors attribute the decrease in the lifetime of the transient absorption signal to charge scavenging by DCBQ from delocalized charge-transfer states of peripheral chlorophylls of isolated PSI complexes and PSI in cyanobacterial cells.[75] Interestingly, they observe in isolated PSI complexes a similar decrease in the transient absorption lifetime upon addition of MV. These results suggest that alternative CS paths from outer chlorophylls could lead to dynamics that does not follow the usual trapping in the RC and thus may have different time scales. However, we find it difficult to explain the complete lack of population dynamics within 450 fs on the basis of MV outer chlorophyll charge scavenging, especially as the latter takes place in a picosecond time scale. To test these hypotheses, future developments in the photoelectrochemical setup are necessary. They include the use of larger, physiologically relevant redox carriers of PSI like its cognate proteins (plastocyanin, cytochromes, ferredoxin) that exchange charge selectively with PSI redox cofactors and thus exclude the possibility of unspecific charge draining.

CONCLUSIONS

Based on the combination of photoelectrochemical current detection (PEC) and two-dimensional electronic spectroscopy (2DES), we proposed the novel PEC2DES technique, which gives direct access to the biologically relevant charge separation process and associated excitation−detection maps. Further-

https://doi.org/10.1021/acsami.4c03652
ACS Appl. Mater. Interfaces 2024, 16, 43451−43461

more, we validated the proof-of-concept of the PEC2DES technique on a biological multichromophoric system, namely, the PSI-LHCI pigment−protein complex of plants, demonstrating its suitability for the extraction of the nonlinear response. In particular, the unidirectional orientation of the PSI-LHCI monolayer on a transparent metal electrode, the choice of redox mediators, and their concentration yield submillisecond transient photoelectrochemical currents of magnitude in the range of 100 $\mu A \cdot cm^{-2}$ that are stable for hours and allow the long-time signal integration required by 2DES experiments.

The overlap between the linear component of the PEC2DES signal and the absorption spectra of the sample demonstrates that PSI-LHCI complexes are responsible for PEC2DES results. However, global analysis does not detect any population dynamics within a delay time of 450 fs. Although this result is against previous optically detected 2DES experiments, it aligns with recent findings in the fluorescence-detected 2DES of LH2 complexes showing a reduced contrast in the energy transfer kinetics along t_2.[74] This difference can be explained by the different nature of the excitation scheme, the presence of a single CS site in the multichromophoric system, and the time scale of the electrochemical detection. Under these conditions, the population dynamics is hidden by the incoherent mixing contribution that dominates the nonlinear response.[69,70] According to the incoherent mixing interpretation, coherent oscillations should also be hidden along delay time t_2. However, the global analysis reveals an oscillatory behavior depicted in the 2D-CAS map. The relative frequency, around 750 cm^{-1}, is compatible with a vibrational mode coupled to the optical transition of chlorophyll *a*. These conflicting results indicate that the incoherent mixing effect may not yet be fully understood.

Future developments and applications of PEC2DES follow two distinct paths. On the one hand, it is necessary to identify suitable samples in which the effect of incoherent mixing is minimized, either because of a lower number of chromophores or because of the presence of delocalization.[70,74] In this case, isolated reaction centers are promising candidates for this technique. On the other hand, it is necessary to find experimental strategies to directly reduce the amount of incoherent mixing in the nonlinear signal. This represents a collaborative effort to pursue along with other action-detected techniques. Indeed, the recent proposal to use time[65,67,76] and frequency[77] gating in fluorescence-detected 2DES moves in this direction.

■ ASSOCIATED CONTENT

Supporting Information

The Supporting Information is available free of charge at https://pubs.acs.org/doi/10.1021/acsami.4c03652.

PSI-LHCI complex purification; Au-pIQA-cys-PSI-LHCI electrode preparation; AFM characterization of the Au-pIQA-cys-PSI-LHCI biohybrid electrode; acquisition and setup details; phase modulation; Dazzler intensity artifact; incoherent mixing, linear reconstruction; incoherent mixing, evolution along t_2; custom electrochemical cell design; and pulse compression (PDF)

■ AUTHOR INFORMATION

Corresponding Authors

Niek F. van Hulst − *ICFO - Institut de Ciències Fotòniques, The Barcelona Institute of Science and Technology, Castelldefels, Barcelona 08860, Spain; ICREA - Institució Catalana de Recerca i Estudis Avançats, Barcelona 08010, Spain;* orcid.org/0000-0003-4630-1776; Email: niek.vanhulst@icfo.eu

Pau Gorostiza − *Institute for Bioengineering of Catalonia (IBEC), The Barcelona Institute of Science and Technology, Barcelona 08028, Spain; ICREA - Institució Catalana de Recerca i Estudis Avançats, Barcelona 08010, Spain; CIBER-BBN, Barcelona 08028, Spain;* orcid.org/0000-0002-7268-5577; Email: pau@icrea.cat

Authors

Manuel López-Ortiz − *Institute for Bioengineering of Catalonia (IBEC), The Barcelona Institute of Science and Technology, Barcelona 08028, Spain*

Luca Bolzonello − *ICFO - Institut de Ciències Fotòniques, The Barcelona Institute of Science and Technology, Castelldefels, Barcelona 08860, Spain;* orcid.org/0000-0003-0893-5743

Matteo Bruschi − *Dipartimento di Scienze Chimiche, Università degli Studi di Padova, Padova 35131, Italy;* orcid.org/0000-0001-7838-0363

Elisa Fresch − *Dipartimento di Scienze Chimiche, Università degli Studi di Padova, Padova 35131, Italy*

Elisabetta Collini − *Dipartimento di Scienze Chimiche, Università degli Studi di Padova, Padova 35131, Italy;* orcid.org/0000-0002-1019-9100

Chen Hu − *Biophysics of Photosynthesis, Department of Physics and Astronomy, Faculty of Sciences, Vrije Universiteit Amsterdam, Amsterdam, HV 1081, The Netherlands*

Roberta Croce − *Biophysics of Photosynthesis, Department of Physics and Astronomy, Faculty of Sciences, Vrije Universiteit Amsterdam, Amsterdam, HV 1081, The Netherlands;* orcid.org/0000-0003-3469-834X

Complete contact information is available at: https://pubs.acs.org/10.1021/acsami.4c03652

Author Contributions

$^{\nabla}$M.L.-O. and L.B. contributed equally.

Notes

The authors declare no competing financial interest.

■ ACKNOWLEDGMENTS

E.C. acknowledges the financial support of the MIUR PRIN2017 (grant 2017A4XRCA). This research received funding from the Ignite Programme of BIST, the European Union Research and Innovation Programme Horizon 2020−DEEPER (ICT-36-2020, grant agreement 101016787), the Agency for Management of University and Research Grants (CERCA Programme; 2017-SGR-1442 project), the Ministry of Science and Innovation DEEP RED grant PID2019-111493RB-I00 funded by MCIN/AEI/10.13039/501100011033, and the Commission for Universities and Research of the Department of Innovation, Universities, and Enterprise of the Government of Catalonia-AGAUR (IU16-011508) and was cofinanced by the European Union Regional Development Fund within the framework of the ERDF/FEDER Operational Program of Catalonia 2014−2020 with a

grant of 50% of total eligible cost. N.F.v.H. acknowledges the financial support by the European Commission (ERC Advanced Grant 101054846-FastTrack), the MCIN/AEI projects PID2021-123814OB-I00 and TED2021-129241B−I00, the "Severo Ochoa" program for Centres of Excellence in R&D CEX2019-000910-S, Fundació Privada Cellex, Fundació Privada Mir-Puig, and the Generalitat de Catalunya through the CERCA program. L.B. received funding from the ICFO Clean Planet Program supported by Fundació Joan Ribas Araquistain (FJRA).

REFERENCES

(1) Croce, R.; Van Amerongen, H. Light-Harvesting in Photosystem I. *Photosynth. Res.* **2013**, *116* (2−3), 153−166.
(2) Chitnis, P. R. PHOTOSYSTEM I: Function and Physiology. *Annu. Rev. Plant Physiol. Plant Mol. Biol.* **2001**, *52*, 593−626.
(3) Croce, R.; van Amerongen, H. Light Harvesting in Oxygenic Photosynthesis: Structural Biology Meets Spectroscopy. *Science* **2020**, *369* (6506), No. eaay2058.
(4) Wu, D. Y.; Li, J. F.; Ren, B.; Tian, Z. Q. Electrochemical Surface-Enhanced Raman Spectroscopy of Nanostructures. *Chem. Soc. Rev.* **2008**, *37* (5), 1025−1041.
(5) Lynk, T. P.; Sit, C. S.; Brosseau, C. L. Electrochemical Surface-Enhanced Raman Spectroscopy as a Platform for Bacterial Detection and Identification. *Anal. Chem.* **2018**, *90* (21), 12639−12646.
(6) Griffin, P. J.; Charette, B. J.; Burke, J. H.; Vura-Weis, J.; Schaller, R. D.; Gosztola, D. J.; Olshansky, L. Toward Improved Charge Separation through Conformational Control in Copper Coordination Complexes. *J. Am. Chem. Soc.* **2022**, *144* (27), 12116−12126.
(7) Hung, S. F.; Wu, F. Y.; Lu, Y. H.; Lee, T. J.; Tsai, H. J.; Chen, P. H.; Lin, Z. Y.; Chen, G. L.; Huang, W. Y.; Zeng, W. J. Operando X-Ray Absorption Spectroscopic Studies of the Carbon Dioxide Reduction Reaction in a Modified Flow Cell. *Catal. Sci. Technol.* **2022**, *12* (9), 2739−2743.
(8) Iwasita, T.; Nart, F. C. In Situ Infrared Spectroscopy at Electrochemical Interfaces. *Prog. Surf. Sci.* **1997**, *55* (4), 271−340.
(9) Pande, N.; Chandrasekar, S. K.; Lohse, D.; Mul, G.; Wood, J. A.; Mei, B. T.; Krug, D. Electrochemically Induced pH Change: Time-Resolved Confocal Fluorescence Microscopy Measurements and Comparison with Numerical Model. *J. Phys. Chem. Lett.* **2020**, *11* (17), 7042−7048.
(10) Tassy, B.; Dauphin, A. L.; Man, H. M.; Le Guenno, H.; Lojou, E.; Bouffier, L.; De Poulpiquet, A. In Situ Fluorescence Tomography Enables a 3D Mapping of Enzymatic O2 Reduction at the Electrochemical Interface. *Anal. Chem.* **2020**, *92* (10), 7249−7256.
(11) Bouffier, L.; Doneux, T. Coupling Electrochemistry with in Situ Fluorescence (Confocal) Microscopy. *Curr. Opin. Electrochem.* **2017**, *6* (1), 31−37.
(12) Timoshenko, J.; Roldan Cuenya, B. R. In Situ/Operando Electrocatalyst Characterization by X-Ray Absorption Spectroscopy. *Chem. Rev.* **2021**, *121* (2), 882−961.
(13) Petersen, H.; Weidenthaler, C. A Review of Recent Developments for the in Situ/Operando Characterization of Nanoporous Materials. *Inorg. Chem. Front.* **2022**, *9* (16), 4244−4271.
(14) Liu, D.; Shadike, Z.; Lin, R.; Qian, K.; Li, H.; Li, K.; Wang, S.; Yu, Q.; Liu, M.; Ganapathy, S.; Qin, X.; Yang, Q.-H.; Wagemaker, M.; Kang, F.; Yang, X.-Q.; Li, B. Review of Recent Development of in Situ/Operando Characterization Techniques for Lithium Battery Research. *Adv. Mater.* **2019**, *31* (28), No. 1806620.
(15) Heitmüller, J.; Eckstein, K.; Renner, R.; Stolte, M.; Hertel, T.; Würthner, F.; Brixner, T. Coherent Two-Dimensional Electronic Spectroelectrochemistry. *Spectrochim. Acta A Mol. Biomol. Spectrosc.* **2021**, *253*, No. 119567.
(16) Zhang, B.; Sun, L. Artificial Photosynthesis: Opportunities and Challenges of Molecular Catalysts. *Chem. Soc. Rev.* **2019**, *48* (7), 2216−2264.
(17) Meneghin, E.; Biscaglia, F.; Volpato, A.; Bolzonello, L.; Pedron, D.; Frezza, E.; Ferrarini, A.; Gobbo, M.; Collini, E. Biomimetic Nanoarchitectures for Light Harvesting: Self-Assembly of Pyropheophorbide-Peptide Conjugates. *J. Phys. Chem. Lett.* **2020**, *11* (19), 7972−7980.
(18) Ennist, N. M.; Zhao, Z.; Stayrook, S. E.; Discher, B. M.; Dutton, P. L.; Moser, C. C. De Novo Protein Design of Photochemical Reaction Centers. *Nat. Commun.* **2022**, *13* (1), 4937.
(19) Hancock, A. M.; Swainsbury, D. J. K.; Meredith, S. A.; Morigaki, K.; Hunter, C. N.; Adams, P. G. Enhancing the Spectral Range of Plant and Bacterial Light-Harvesting Pigment-Protein Complexes with Various Synthetic Chromophores Incorporated into Lipid Vesicles. *J. Photochem. Photobiol., B* **2022**, *237*, No. 112585.
(20) Hancock, A. M.; Son, M.; Nairat, M.; Wei, T.; Jeuken, L. J. C.; Duffy, C. D. P.; Schlau-Cohen, G. S.; Adams, P. G. Ultrafast Energy Transfer between Lipid-Linked Chromophores and Plant Light-Harvesting Complex II. *Phys. Chem. Chem. Phys.* **2021**, *23* (35), 19511−19524.
(21) Liu, J.; Friebe, V. M.; Frese, R. N.; Jones, M. R. Polychromatic solar energy conversion in pigment-protein chimeras that unite the two kingdoms of (bacterio)chlorophyll-based photosynthesis. *Nat. Commun.* **2020**, *11* (1), 1542.
(22) Sardjan, A. S.; Westerman, F. P.; Ogilvie, J. P.; Jansen, T. L. C. Observation of Ultrafast Coherence Transfer and Degenerate States with Polarization-Controlled Two-Dimensional Electronic Spectroscopy. *J. Phys. Chem. B* **2020**, *124* (42), 9420−9427.
(23) Nishita, M.; Park, S.-Y.; Nishio, T.; Kamizaki, K.; Wang, Z.; Tamada, K.; Takumi, T.; Hashimoto, R.; Otani, H.; Pazour, G. J.; Hsu, V. W.; Minami, Y. Ror2 Signaling Regulates Golgi Structure and Transport through IFT20 for Tumor Invasiveness. *Sci. Rep.* **2017**, *7* (1), 1.
(24) Gelzinis, A.; Augulis, R.; Butkus, V.; Robert, B.; Valkunas, L. Two-Dimensional Spectroscopy for Non-Specialists. *Biochim. Biophys. Acta Bioenerg.* **2019**, *1860* (4), 271−285.
(25) Cao, J.; Cogdell, R. J.; Coker, D. F.; Duan, H. G.; Hauer, J.; Kleinekathöfer, U.; Jansen, T. L. C.; Mančal, T.; Miller, R. J. D.; Ogilvie, J. P.; Prokhorenko, V. I.; Renger, T.; Tan, H. S.; Tempelaar, R.; Thorwart, M.; Thyrhaug, E.; Westenhoff, S.; Zigmantas, D. Quantum biology revisited. *Sci. Adv.* **2020**, *6*, No. eaaz4888.
(26) Bolzonello, L.; Volpato, A.; Meneghin, E.; Collini, E. Versatile Setup for High-Quality Rephasing, Non-Rephasing, and Double Quantum 2D Electronic Spectroscopy. *J. Opt. Soc. Am. B* **2017**, *34* (6), 1223.
(27) Brixner, T.; Mancal, T.; Stiopkin, I. V.; Fleming, G. R. Phase-Stabilized Two-Dimensional Electronic Spectroscopy. *J. Chem. Phys.* **2004**, *121* (9), 4221−4236.
(28) Tekavec, P. F.; Myers, J. A.; Lewis, K. L. M.; Ogilvie, J. P. Two-Dimensional Electronic Spectroscopy with a Continuum Probe. *Opt. Lett.* **2009**, *34* (9), 1390−1392.
(29) Damtie, F. A.; Wacker, A.; Pullerits, T.; Karki, K. J. Two-Dimensional Action Spectroscopy of Excitonic Systems: Explicit Simulation Using a Phase-Modulation Technique. *Phys. Rev. A (Coll Park)* **2017**, *96* (5), No. 053830.
(30) Karki, K. J.; Widom, J. R.; Seibt, J.; Moody, I.; Lonergan, M. C.; Pullerits, T.; Marcus, A. H. Coherent Two-Dimensional Photocurrent Spectroscopy in a PbS Quantum Dot Photocell. *Nat. Commun.* **2014**, *5* (1), 5869.
(31) Bolzonello, L.; Bernal-Texca, F.; Gerling, L. G.; Ockova, J.; Collini, E.; Martorell, J.; Van Hulst, N. F. Photocurrent-Detected 2D Electronic Spectroscopy Reveals Ultrafast Hole Transfer in Operating PM6/Y6 Organic Solar Cells. *J. Phys. Chem. Lett.* **2021**, *12* (16), 3983−3988.
(32) Goetz, S.; Li, D.; Kolb, V.; Pflaum, J.; Brixner, T. Coherent Two-Dimensional Fluorescence Micro-Spectroscopy. *Opt. Express* **2018**, *26* (4), 3915−3925.
(33) Tiwari, V.; Matutes, Y. A.; Gardiner, A. T.; Jansen, T. L. C.; Cogdell, R. J.; Ogilvie, J. P. Spatially-Resolved Fluorescence-Detected Two-Dimensional Electronic Spectroscopy Probes Varying Excitonic Structure in Photosynthetic Bacteria. *Nat. Commun.* **2018**, *9* (1), 4219.

https://doi.org/10.1021/acsami.4c03652
ACS Appl. Mater. Interfaces 2024, 16, 43451−43461

(34) Mueller, S.; Draeger, S.; Ma, X.; Hensen, M.; Kenneweg, T.; Pfeiffer, W.; Brixner, T. Fluorescence-Detected Two-Quantum and One-Quantum-Two-Quantum 2D Electronic Spectroscopy. *J. Phys. Chem. Lett.* **2018**, *9* (8), 1964−1969.
(35) Malý, P.; Lüttig, J.; Mueller, S.; Schreck, M. H.; Lambert, C.; Brixner, T. Coherently and Fluorescence-Detected Two-Dimensional Electronic Spectroscopy: Direct Comparison on Squaraine Dimers. *Phys. Chem. Chem. Phys.* **2020**, *22* (37), 21222−21237.
(36) Karki, K. J.; Chen, J.; Sakurai, A.; Shi, Q.; Gardiner, A. T.; Kühn, O.; Cogdell, R. J.; Pullerits, T. Before Förster. Initial Excitation in Photosynthetic Light Harvesting. *Chem. Sci.* **2019**, *10* (34), 7923−7928.
(37) Perdomo-Ortiz, A.; Widom, J. R.; Lott, G. A.; Aspuru-Guzik, A.; Marcus, A. H. Conformation and Electronic Population Transfer in Membrane-Supported Self-Assembled Porphyrin Dimers by 2D Fluorescence Spectroscopy. *J. Phys. Chem. B* **2012**, *116* (35), 10757−10770.
(38) Golbeck, J. H. *Photosystem I*; Springer: Netherlands, 2006.
(39) Wientjes, E.; Croce, R. PMS: Photosystem I Electron Donor or Fluorescence Quencher. *Photosynth. Res.* **2012**, *111* (1−2), 185−191.
(40) Nawrocki, W. J.; Jones, M. R.; Frese, R. N.; Croce, R.; Friebe, V. M. *In Situ* Time-Resolved Spectroelectrochemistry Reveals Limitations of Biohybrid Photoelectrode Performance. *Joule* **2023**, *7* (3), 529−544.
(41) Baker, D. R.; Manocchi, A. K.; Lamicq, M. L.; Li, M.; Nguyen, K.; Sumner, J. J.; Bruce, B. D.; Lundgren, C. A. Comparative Photoactivity and Stability of Isolated Cyanobacterial Monomeric and Trimeric Photosystem I. *J. Phys. Chem. B* **2014**, *118* (10), 2703−2711.
(42) Manocchi, A. K.; Baker, D. R.; Pendley, S. S.; Nguyen, K.; Hurley, M. M.; Bruce, B. D.; Sumner, J. J.; Lundgren, C. A. Photocurrent Generation from Surface Assembled Photosystem I on Alkanethiol Modified Electrodes. *Langmuir* **2013**, *29* (7), 2412−2419.
(43) McCoy, D. E.; Feo, T.; Harvey, T. A.; Prum, R. O. Structural Absorption by Barbule Microstructures of Super Black Bird of Paradise Feathers. *Nat. Commun.* **2018**, *9* (1), 1.
(44) Zhao, F.; Ruff, A.; Rögner, M.; Schuhmann, W.; Conzuelo, F. Extended Operational Lifetime of a Photosystem-Based Bioelectrode. *J. Am. Chem. Soc.* **2019**, *141* (13), 5102−5106.
(45) Zhang, W.; Liu, M.; Zhang, P.; Yu, F.; Lu, S.; Li, P.; Zhou, J. Effects of Paraquat on Photosynthetic Pigments, Antioxidant Enzymes, and Gene Expression in Chlorella Pyrenoidosa under Mixotrophic Compared with Autotrophic Conditions. *Arch. Environ. Contam. Toxicol.* **2014**, *67* (4), 593−600.
(46) Forouzesh, A.; Zand, E.; Soufizadeh, S.; Samadi Foroushani, S. Classification of Herbicides according to Chemical Family for Weed Resistance Management Strategies−An Update. *Weed Res.* **2015**, *55* (4), 334−358.
(47) Zhao, F.; Plumeré, N.; Nowaczyk, M. M.; Ruff, A.; Schuhmann, W.; Conzuelo, F. Interrogation of a PS1-Based Photocathode by means of Scanning Photoelectrochemical Microscopy. *Small* **2017**, *13* (26), No. 1604093.
(48) López-Ortiz, M.; Zamora, R. A.; Antinori, M. E.; Remesh, V.; Hu, C.; Croce, R.; Van Hulst, N. F.; Gorostiza, P. Fast Photo-Chrono-Amperometry of Photosynthetic Complexes for Biosensors and Electron Transport Studies. *ACS Sens.* **2021**, *6* (2), 581−587.
(49) Buesen, D.; Hoefer, T.; Zhang, H.; Plumeré, N. A Kinetic Model for Redox-Active Film Based Biophotoelectrodes. *Faraday Discuss.* **2019**, *215*, 39−53.
(50) Gordiichuk, P.; Pesce, D.; Ocampo, O. E. C.; Marcozzi, A.; Wetzelaer, G.-J. A. H.; Paul, A.; Loznik, M.; Gloukhikh, E.; Richter, S.; Chiechi, R. C.; Herrmann, A. Orientation and Incorporation of Photosystem I in Bioelectronics Devices Enabled by Phage Display. *Adv. Sci.* **2017**, *4*, No. 1600393.
(51) López-Ortiz, M.; Zamora, R. A.; Giannotti, M. I.; Hu, C.; Croce, R.; Gorostiza, P. Distance and Potential Dependence of Charge Transport through the Reaction Center of Individual Photosynthetic Complexes. *Small* **2022**, *18* (7), No. e2104366.
(52) Volpato, A.; Bolzonello, L.; Meneghin, E.; Collini, E. Global Analysis of Coherence and Population Dynamics in 2D Electronic Spectroscopy. *Opt. Express* **2016**, *24* (21), 24773−24785.
(53) Paleček, D.; Edlund, P.; Gustavsson, E.; Westenhoff, S.; Zigmantas, D. Potential Pitfalls of the Early-Time Dynamics in Two-Dimensional Electronic Spectroscopy. *J. Chem. Phys.* **2019**, *151* (2), No. 024201.
(54) Turner, D. B.; Wilk, K. E.; Curmi, P. M. G.; Scholes, G. D. Comparison of Electronic and Vibrational Coherence Measured by Two-Dimensional Electronic Spectroscopy. *J. Phys. Chem. Lett.* **2011**, *2* (15), 1904.
(55) Tang, J.; Norrist, J. R. Linear Prediction z-Transform (LPZ) Method, Padé Rational Approximation, and the Burg Maximum Entropy Extrapolation. *J. Magn. Reson. (1969)* **1988**, *78* (1), 23−30.
(56) Meneghin, E.; Leonardo, C.; Volpato, A.; Bolzonello, L.; Collini, E. Mechanistic Insight into Internal Conversion Process within Q-Bands of Chlorophyll a. *Sci. Rep.* **2017**, *7* (1), 11389.
(57) Meneghin, E.; Pedron, D.; Collini, E. Raman and 2D Electronic Spectroscopies: A Fruitful Alliance for the Investigation of Ground and Excited State Vibrations in Chlorophyll a. *Chem. Phys.* **2018**, *514*, 132−140.
(58) Senlik, S. S.; Policht, V. R.; Ogilvie, J. P. Two-Color Nonlinear Spectroscopy for the Rapid Acquisition of Coherent Dynamics. *J. Phys. Chem. Lett.* **2015**, *6* (13), 2413.
(59) Zhou, C.; Diers, J. R.; Bocian, D. F. Qy -Excitation Resonance Raman Spectra of Chlorophyll a and Related Complexes. Normal Mode Characteristics of the Low-Frequency Vibrations. *J. Phys. Chem. B* **1997**, *101* (46), 9635−9644.
(60) Russo, M.; Casazza, A. P.; Cerullo, G.; Santabarbara, S.; Maiuri, M. Direct Evidence for Excitation Energy Transfer Limitations Imposed by Low-Energy Chlorophylls in Photosystem I-Light Harvesting Complex I of Land Plants. *J. Phys. Chem. B* **2021**, *125* (14), 3566−3573.
(61) Akhtar, P.; Zhang, C.; Liu, Z.; Tan, H. S.; Lambrev, P. H. Excitation Transfer and Trapping Kinetics in Plant Photosystem I Probed by Two-Dimensional Electronic Spectroscopy. *Photosynth. Res.* **2018**, *135* (1−3), 239−250.
(62) Akhtar, P.; Caspy, I.; Nowakowski, P. J.; Malavath, T.; Nelson, N.; Tan, H. S.; Lambrev, P. H. Two-Dimensional Electronic Spectroscopy of a Minimal Photosystem I Complex Reveals the Rate of Primary Charge Separation. *J. Am. Chem. Soc.* **2021**, *143* (36), 14601−14612.
(63) Russo, M.; Casazza, A. P.; Cerullo, G.; Santabarbara, S.; Maiuri, M. Ultrafast Excited State Dynamics in the Monomeric and Trimeric Photosystem I Core Complex of Spirulina Platensis Probed by Two-Dimensional Electronic Spectroscopy. *J. Chem. Phys.* **2022**, *156* (16), 164202.
(64) Malý, P.; Lüttig, J.; Mueller, S.; Schreck, M. H.; Lambert, C.; Brixner, T. Coherently and Fluorescence-Detected Two-Dimensional Electronic Spectroscopy: Direct Comparison on Squaraine Dimers. *Phys. Chem. Chem. Phys.* **2020**, *22* (37), 21222−21237.
(65) Malý, P.; Mančal, T. Signatures of Exciton Delocalization and Exciton−Exciton Annihilation in Fluorescence-Detected Two-Dimensional Coherent Spectroscopy. *J. Phys. Chem. Lett.* **2018**, *9* (19), 5654−5659.
(66) Mukamel, S. *Principles of Nonlinear Optical Spectroscopy*; Oxford University Press, 1995.
(67) Kunsel, T.; Tiwari, V.; Matutes, Y. A.; Gardiner, A. T.; Cogdell, R. J.; Ogilvie, J. P.; Jansen, T. L. C. Simulating Fluorescence-Detected Two-Dimensional Electronic Spectroscopy of Multichromophoric Systems. *J. Phys. Chem. B* **2019**, *123* (2), 394−406.
(68) Kühn, O.; Mančal, T.; Pullerits, T. Interpreting Fluorescence Detected Two-Dimensional Electronic Spectroscopy. *J. Phys. Chem. Lett.* **2020**, *11* (3), 838−842.
(69) Bruschi, M.; Bolzonello, L.; Gallina, F.; Fresch, B. Unifying Nonlinear Response and Incoherent Mixing in Action-2D Electronic Spectroscopy. *J. Phys. Chem. Lett.* **2023**, *14*, 6872.
(70) Bolzonello, L.; Bruschi, M.; Fresch, B.; van Hulst, N. F. Nonlinear Optical Spectroscopy of Molecular Assemblies: What Is

Gained and Lost in Action Detection? *J. Phys. Chem. Lett.* **2023**, *14* (50), 11438−11446.
(71) Wulf, K.; Trissl, H.-W. Competition between Annihilation and Trapping Leads to Strongly Reduced Yields of Photochemistry under Ps-Flash Excitation. *Photosynth Res.* **1996**, *48* (1−2), 255−262.
(72) Grégoire, P.; Srimath Kandada, A. R.; Vella, E.; Tao, C.; Leonelli, R.; Silva, C. Incoherent Population Mixing Contributions to Phase-Modulation Two-Dimensional Coherent Excitation Spectra. *J. Chem. Phys.* **2017**, *147* (11), 114201.
(73) Bargigia, I.; Gutiérrez-Meza, E.; Valverde-Chávez, D. A.; Marques, S. R.; Srimath Kandada, A. R.; Silva, C. Identifying Incoherent Mixing Effects in the Coherent Two-Dimensional Photocurrent Excitation Spectra of Semiconductors. *J. Chem. Phys.* **2022**, *157* (20), 204202.
(74) Javed, A.; Lüttig, J.; Charvátová, K.; Sanders, S. E.; Willow, R.; Zhang, M.; Gardiner, T. A.; P., Malý; Ogilvie, J. P. Photosynthetic energy transfer: missing in action (detected spectroscopy)?. *arXiv preprint arXiv:2406.06784.* 2024.
(75) Baikie, T. K.; Wey, L. T.; Lawrence, J. M.; Medipally, H.; Reisner, E.; Nowaczyk, M. M.; Friend, R. H.; Howe, C. J.; Schnedermann, C.; Rao, A.; Zhang, J. Z. Photosynthesis Re-Wired on the Pico- Second Timescale. *Nature* **2023**, *615* (7954), 836−840.
(76) Bruschi, M.; Gallina, F.; Fresch, B. Simulating Action-2D Electronic Spectroscopy of Quantum Dots: Insights on the Exciton and Biexciton Interplay from Detection-Mode and Time-Gating. *Phys. Chem. Chem. Phys.* **2022**, *24* (45), 27645−27659.
(77) Yang, J.; Gelin, M. F.; Chen, L.; Šanda, F.; Thyrhaug, E.; Hauer, J. Two-Dimensional Fluorescence Excitation Spectroscopy: A Novel Technique for Monitoring Excited-State Photophysics of Molecular Species with High Time and Frequency Resolution. *J. Chem. Phys.* **2023**, *159* (7), No. 074201.

https://doi.org/10.1021/acsami.4c03652
ACS Appl. Mater. Interfaces 2024, 16, 43451−43461